Magnetic Resonance in Medicine 65:1711–1717 (2011)

Novel 16-Channel Receive Coil Array for Accelerated Upper Airway MRI at 3 Tesla

Yoon-Chul Kim,[1]* Cecil E. Hayes,[2] Shrikanth S. Narayanan,[1] and Krishna S. Nayak[1]

Upper airway MRI can provide a noninvasive assessment of speech and swallowing disorders and sleep apnea. Recent work has demonstrated the value of high-resolution three-dimensional imaging and dynamic two-dimensional imaging and the importance of further improvements in spatio-temporal resolution. The purpose of the study was to describe a novel 16-channel 3 Tesla receive coil that is highly sensitive to the human upper airway and investigate the performance of accelerated upper airway MRI with the coil. In three-dimensional imaging of the upper airway during static posture, 6-fold acceleration is demonstrated using parallel imaging, potentially leading to capturing a whole three-dimensional vocal tract with 1.25 mm isotropic resolution within 9 sec of sustained sound production. Midsagittal spiral parallel imaging of vocal tract dynamics during natural speech production is demonstrated with 2 × 2 mm^2 in-plane spatial and 84 ms temporal resolution. Magn Reson Med 65:1711–1717, 2011.

Key words: upper airway MRI; RF coil design; parallel imaging; rapid imaging

MRI is a powerful tool for the noninvasive assessment of upper airway anatomy and function. Upper airway MRI has been used to investigate the feasibility of clinical assessments in patients with obstructive sleep apnea (1,2) and swallowing disorders (3). In sleep apnea studies, rapid volumetric imaging is desirable for identifying the sites of the narrowing or occlusion of the airway and measuring its volume. In swallowing studies, high temporal resolution real-time MRI is desirable for the evaluation of swallowing disorders. This enables improved assessment of the dynamics of a bolus of food without introducing motion artifacts.

Rapid upper airway MRI is also valuable for basic research into human speech production. In such studies, volumetric coverage is typically obtained during sustained sound production, using a two-dimensional (2D) multislice (4), or native three-dimensional (3D) acquisition (5). Tract dynamics (e.g., movement of the tongue and velum) is typically assessed using real-time acquisition of a single 2D slice (e.g., midsagittal) (6). An objective and quantitative knowledge of the orchestration of articulatory activity that creates speech is a necessary element in understanding of human communication. A perennial challenge in speech production research is the ability to examine 3D real-time changes in the shaping of the vocal tract. Spatio-temporal information about speech movements is critical not only to understanding and modeling the speech production process but also to a thorough understanding of speech acoustics; this in turn has significant implications for developing applications of machine synthesis and recognition of speech.

From a translational perspective, understanding speech production deficits due to neurological damage or other disease etiology directly from articulation details (versus what is offered by speech acoustic recordings) is critical to assess and plan treatment. For example, people with certain neurological disease (e.g., apraxia) are known to exhibit speech timing patterns differing from neurologically unimpaired speakers [see articulatory data in Ref. (7)]. The fact that both irregularities in the implementation of linguistic prosody and irregularities in articulatory timing patterns occur in neurologically impaired populations implies that investigation of the influence of prosodic structure on articulatory timing may illuminate the general question of how language-specific knowledge is related to motor control. Rapid upper airway MRI offers tools to look at clinical disorders in a new way.

A variety of pulse sequences and image reconstruction techniques have been applied to improve the spatio-temporal resolution of upper airway MRI. Spiral gradient echo imaging techniques have been shown to be effective at capturing vocal tract dynamics during natural speech production (8,9). Improved spatio-temporal resolution imaging has been demonstrated in the assessment of swallowing disorder using parallel imaging on a standard 12-channel head and neck array coil (10). However, a design and use of dedicated multiple channel receiver coil array which is highly sensitive to the upper airway anatomy has not been reported in the literature. In this manuscript, a novel 3 Tesla 16-channel upper airway coil is described and its performance is demonstrated. In volunteers, the signal-to-noise ratio (SNR) and parallel imaging *g*-factor values are compared over the upper airway regions of interest (ROIs) in the midsagittal slice. The 3D parallel imaging of the upper airway is demonstrated to investigate the feasibility of high resolution accelerated upper airway MRI during sustained sound production. Real-time spiral acquisition and parallel imaging reconstruction is applied to capture vocal tract dynamics during natural sound production and is demonstrated with 2.0 × 2.0 mm^2 spatial and 84 msec temporal resolution.

[1]Ming Hsieh Department of Electrical Engineering, University of Southern California, Los Angeles, California, USA.
[2]Department of Radiology, University of Washington, Seattle, Washington, USA.
Grant sponsor: NIH; Grant number: R01-DC007124
*Correspondence to: Yoon-Chul Kim, MS., 3740 McClintock Ave, EEB 400, University of Southern California, Los Angeles, CA 90089-2564.
E-mail: yoonckim@usc.edu
Received 10 August 2010; revised 1 November 2010; accepted 7 November 2010.
DOI 10.1002/mrm.22742
Published online 16 December 2010 in Wiley Online Library (wileyonlinelibrary.com).

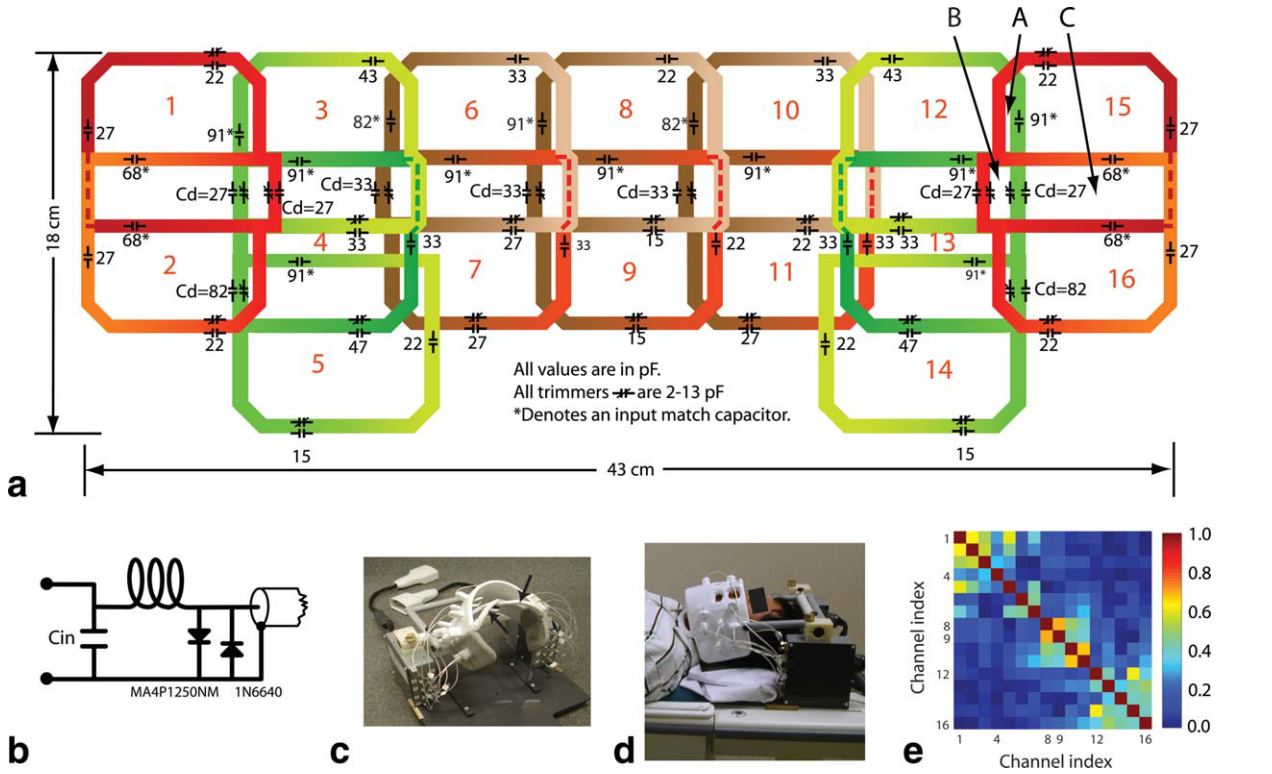

FIG. 1. The 16-channel upper airway receive coil array. **(a):** Coil layout. Individual coil elements are overlapped with their neighboring coil elements to minimize mutual inductive coupling. The two lower coil elements, which correspond to the arrows in (c), extend down the side of the neck region to improve SNR of the lower airway. Channel indices are indicated by the red colored numbers. **(b):** Input circuit diagram. **(c):** Photograph of the 16-channel coil. Each coil element is connected to a preamplifier. A pivoting cross bar is supported by the two preamplifier boxes and holds an adjustable cantilever connected to the coil array. The coil array can be held close to the face or folded up and back to permit patient entry and exit. **(d):** Side view of the 16-channel coil placed on a supine volunteer. **(e):** Noise correlation matrix from one representative volunteer.

MATERIALS AND METHODS

Coil Design and Construction

The desired upper airway field-of-view (FOV) extends in the superior-inferior (S-I) direction from above the hard palate down the throat to the level of the third cervical vertebra (C3) and in the anterior-posterior (A-P) direction, from several centimeters in front of the lips to the anterior surface of the cervical spine.

Our coil configuration consists of seven subgroups of elements: five longitudinal pairs and two longitudinal triplets (see Fig. 1a). The coils in each subgroup share a common conducting element along one edge (uniform color in Fig. 1a) but form two layers along the opposite side (dashed line). The array has an overall dimension of 43 $\times$ 18 cm^2. Fourteen elements have a dimension of 8.2 $\times$ 7.5 cm^2 whereas the third coil of each triplet has a dimension of 8.5 $\times$ 7.5 cm^2. The top two bands of seven coil elements each are mounted on a thin plastic substrate that wraps around the lower face. The third coil of each triplet extends down the side of the neck and is encased in a flexible foam cover that allows it to curve under the chin for a tighter coupling to the neck region (Fig. 1c). The overlaps between neighboring coil elements form three different areas: **A**, **B**, and **C** in Fig. 1a. The contour of the coil elements was adjusted so that area **B** cancels the mutual inductive coupling between diagonal elements. The sum of the areas **A** and **B** cancels the coupling between the circumferentially adjacent coils. The overlap **C** between longitudinally adjacent coil elements is larger than that needed to cancel mutual inductive coupling. For coils spaced along the *z*-direction with the conventional overlap (11), the SNR profile shows two peaks with a valley where the coils intersect. The overlapping area **C** was enlarged to eliminate the valley and give a flat SNR response along the *z*-direction. The resulting excess mutual inductance can be canceled with the decoupling capacitor C_d placed in the common conducting element. In all cases, the coupling between adjacent coil elements could be compensated far below the inherent inductive coupling between nonadjacent coil elements. The individual coil elements were tuned with the trimmer capacitors to give a minimal reactive component to the input impedance when the coils were loaded with a volunteer. The input match capacitor of each element (marked with an asterisk in Fig. 1a) is connected to an input match circuit (Fig. 1b). The pin diode MA4P1250NM provides active blocking during the transmit pulse. The signal diode 1N6640 allows passive blocking if the coil is not plugged into the scanner. The ratio of the unloaded Q to loaded Q for each coil element was deduced from measurements of the coil input impedances. The ratio was taken from the peak values of the resistive component of the input impedance of the unloaded and loaded condition.

Each coil element is connected to a 27 dB-gain, low-input-impedance preamplifier (Rich Spring Technologies, Arcadia, CA) located in a box on either side of the head. Each coaxial cable connecting a coil element and its preamp is fitted with a radiofrequency trap at the input of the preamp to eliminate multiple ground connections to different points on the subgroup's common conductor and to prevent spurious eddy currents in the shields of the coax. The radiofrequency trap consists of three turns of 0.040" semi-rigid coax inside a cylindrical shell made from double-sided Teflon circuit board. The outer surface of the Teflon is etched to form two capacitors between two outer conducting pads and the common inner pad. The outer pads are segmented into many smaller, binary weighted pads connected with small bridges. Each trap was tuned to 127.72 MHz by cutting a sufficient number of the bridges with a file while monitoring its insertion loss with a network analyzer. This construction is an economical way to produce numerous traps that can be fine-tuned without stocking a large number of different values of high voltage capacitors or using expensive variable capacitors.

The preamp boxes are mounted on a base plate that serves as the platform for an adjustable headrest padded with memory foam. The two preamp boxes serve as the base of a pivoting cross bar that holds an adjustable cantilever connected to the facemask coil array. The coil array can be held close to the face (Fig. 1d) or folded up and back to permit patient entry and exit. The outputs of the two preamp boxes were connected to the scanner's input sockets by way of two cables that were each fitted with a single radiofrequency trap. The latter trap consists of two concentric conducting cylinders that are connected at each end by several capacitors in parallel.

In Vivo Experiments

Experiments were performed on a Signa EXCITE HDx 3.0 T scanner (GE Healthcare, Waukesha, WI) with gradients capable of 40 mT/m amplitude and 150 mT/m/msec slew rate. The receiver bandwidth was set to ±125 kHz (i.e., 4 μsec sampling rate) for all studies. The 16-channel coil was placed about 1–2 cm anterior to the tip of the nose in all subjects. Prior to the scan, each subject was screened and provided informed consent in accordance with institutional policy. The noise correlation matrix as a measure of coil coupling was computed by (1) acquiring data with no radiofrequency excitation and (2) calculating noise correlation from every pair of the coil elements as described in Eq. 6 of Ref. (12).

For the SNR and *g*-factor evaluation, 3D volume of the upper airway was acquired in supine position using a 3DFT gradient echo sequence. Imaging parameters were: flip angle = 10°; k_y and k_z phase encoding along A-P and right-left (R-L) directions, respectively; echo time = 2.1 msec; pulse repetition time = 3.9 msec; 1.88 × 1.88 × 2.50 mm^3 spatial resolution; 24 × 24 × 18 cm^3 FOV; pixel dimension = 128 × 128 × 72; scan time = 30 sec. The subjects held their mouth closed without swallowing during each 30 sec scan. We considered a retrospective 1D regular undersampling on a midsagittal slice. The undersampling was along A-P direction. We performed the SNR evaluation of the 16-channel coil by comparing it with widely available single-channel birdcage transmit/receive coil and 8-channel neurovascular (NV) receive coil, and also by comparing the performance of the 16-channel coil among three subjects. The single-channel birdcage coil is cylindrical-shaped with the inner diameter of 28 cm and the length of 38 cm, and usually covers the brain. The 8-channel NV coil consists of a 4-element head array and 4-element neck array: the head array has an inner diameter of 22 cm and length of 33 cm. The neck array has a dimension of 34 × 17 cm^2 in the anterior neck region and a dimension of 44 × 22 cm^2 in the posterior neck region. Eight ROIs (see Fig. 2) were selected manually on a midsagittal scan plane, and the average SNRs were evaluated on each ROI separately. For the data acquired from the 8-channel NV and 16-channel UA coils, the average SNRs were calculated from images in SNR units reconstructed from the B_1-weighted combining method described in Eq. 6 of Ref. (13). Low resolution coil sensitivity maps were calculated from 32 central *k*-space lines by dividing the image at each coil element by the root sum-of-squares image. We compared image quality between one large male and one small female on a midsagittal scan plane after performing parallel imaging reconstruction (14) for reduction factors of R = 2, 3, 4, and 5. Parallel imaging *g*-factors were calculated on a pixel-by-pixel basis as described in Ref. (14).

FIG. 2. Illustration of coil sensitivity and the upper airway regions of interest (ROIs) used in the evaluation of SNR. Shown is a midsagittal image from Subject 3 obtained using the 16-channel upper airway coil. Note that the image has the most highly localized sensitivity over the upper airway. The eight ROIs identified by red contours are numbered as follows: 1—upper lip, 2—lower lip, 3—front tongue, 4—mid tongue, 5—back tongue, 6—palate, 7—velum, and 8—pharyngeal wall. [Color figure can be viewed in the online issue, which is available at wileyonlinelibrary.com.]

High resolution imaging of the 3D vocal tract was demonstrated using a 3DFT gradient echo sequence. Imaging parameters were: 8 cm midsagittal slab excitation, flip angle = 5°; k_y and k_z phase encoding along A-P and R-L

directions, respectively; echo time = 2.1 msec; pulse repetition time = 4.2 msec; 1.25 × 1.25 × 1.25 mm^3 spatial resolution; 20 × 20 × 10 cm^3 FOV; pixel dimension = 160 × 160 × 80; scan time = 54 sec. During each 54 sec scan, the subjects held their mouth open without swallowing. For the evaluation of parallel imaging performance, we considered a retrospective 2D regular undersampling on the k_y and k_z encodes after taking the inverse Fourier transform along the readout direction (i.e., S-I). Sensitivity encoding (SENSE) reconstructions were performed at each axial slice in which coil calibration was performed using the central 32 × 32 (k_y, k_z) encodes.

Real-time upper airway MRI during natural speech sound production was demonstrated on the 16-channel UA coil using a 2D spiral gradient echo sequence. Imaging parameters were: echo time = 1.4 msec, pulse repetition time = 4.0 msec, readout duration = 1.2 msec, slice thickness = 5 mm, flip angle = 10°, FOV = 30 × 30 cm^2, spatial resolution = 2.0 × 2.0 mm^2, image matrix size = 150 × 150. The subject was instructed to repeat "go pee shop okay bow know" during the scan. The angular increment of spiral interleaves in *k*-space was based on the golden-ratio temporal view order (15), which supports a retrospective selection of temporal resolution at any arbitrary time point.

From the 2D spiral datasets, five different acceleration factors of 1.0, 1.6, 2.6, 4.2, and 6.8 were considered in frame reconstruction. Their corresponding numbers of spiral interleaves were 89, 55, 34, 21, and 13 which led to temporal resolution of 356, 220, 136, 84, and 52 msec, respectively. Coil sensitivity calibration was performed by utilizing multicoil data corresponding to fully-sampled temporal window and by dividing the image at each coil element by the root sum-of-squares image. The coil sensitivity maps and noise covariance matrix were applied to image reconstruction. Image reconstruction from the undersampled multicoil spiral data was based on an iterative conjugate gradient algorithm after taking the noise decorrelation steps as described in Ref. (16). Iterations were stopped at the 15th iterate for the acceleration factors of 1.0, 1.6, and 2.6 and at the 20th iterate for the acceleration factors of 4.2, and 6.8 based on Ref. (17). After the reconstruction of the frames, temporal median filtering with a filter length of 5 was applied pixel-by-pixel to successive frames to eliminate residual aliasing artifacts in reconstructed frames (18).

RESULTS

The majority of the $Q_{unloaded}/Q_{loaded}$ ratios ranged from 4 to 6 with a few as high as 8 depending on how closely the array was placed on the subject. Figure 1e shows a noise correlation matrix from a healthy volunteer. The off-diagonal elements in the noise correlation matrix ranged from 0.0029 to 0.7039 with a mean of 0.1738. The maximum noise correlation occurred in a pair of longitudinally adjacent coil elements, which has a relatively larger degree of overlap than a pair of horizontally adjacent coil elements.

Table 1 compares SNR for eight different ROIs with the three different coils on one subject. The 16-channel coil produced highest SNR in every region. Particularly, the average SNR in the lower lip provided an 8.8-fold and 19-fold increase compared to the 8-channel NV coil and birdcage coil, respectively. The 16-channel coil produced the smallest SNR improvement in the pharyngeal wall, 1.5 over the 8-channel coil and 2.0 over the birdcage coil.

Table 1
Average SNR Improvement

	ROI	$SNR_{UA}/SNR_{Birdcage}$	SNR_{UA}/SNR_{NV}
1	Upper lip	11.6	5.2
2	Lower lip	19.0	8.8
3	Front tongue	10.0	5.5
4	Mid tongue	5.4	3.5
5	Back tongue	4.1	2.6
6	Palate	3.2	1.9
7	Velum	2.9	2.0
8	Pharyngeal wall	2.0	1.5

Average SNR was measured in a single subject (33-year-old male) using the 16-channel UA coil, single-channel birdcage coil, and 8-channel NV coil. Eight regions of interest (see Fig. 2) were identified in 2D midsagittal images with 1.88 × 1.88 × 2.50 mm^3 spatial resolution, obtained without the use of parallel imaging. The 16-channel UA coil provided improved intrinsic SNR in all regions of interest.
UA, upper airway; NV, neurovascular.

Table 2 compares SNR ratio for eight different ROIs on three subjects with the 16-channel coil. The maximum SNR ratio from Subject 2 was 3.1, which was far lower than 7.1 and 8.0 from Subject 1 and Subject 3, respectively. This results from the fact that Subject 2 has the relatively smaller head size and the coil array is placed close to the orofacial part of the head.

Figure 3 contains SENSE reconstructed images and *g*-factor maps for $R = 2$ to 5 from one large male (Subject 1) and one small female (Subject 2) using the 16-channel coil. The pharyngeal wall of Subject 1 in Fig. 3a is seen relatively darker than that of Subject 2 in Fig. 3c because of the larger head size of Subject 1 and the geometry of the 16-channel coil. In both subjects the SENSE images up to a reduction factor 4 exhibited good depiction of air-tissue boundaries in the upper airway ROIs as indicated by the red contours in Fig. 3a and c. Note that the spiky artifacts resulting from noise amplification due to sensitivity matrix inversion are observed in the $R = 3$, 4, and 5 SENSE images in both subjects. The mean *g*-factors in the upper airway ROIs were comparable in both subjects for all reduction factors considered.

Figure 4 compares $R = 1$ and $R = 6$ SENSE images on one reformatted midsagittal, four reformatted coronal, and four axial slices. Slice prescriptions for the coronal and axial slices are indicated by the solid lines in Fig. 4a. These slices were chosen because they contain information on the air-tissue boundaries necessary for the extraction of the 3D vocal tract shape (4). Although the $R = 6$ SENSE images are noisier than the $R = 1$ images, they preserve the air-tissue boundary features that are relevant to the measurement of the vocal tract area function.

Figure 5 contains spiral SENSE reconstructed images of the midsagittal slice for five different acceleration factors of 1.0, 1.6, 2.6, and 4.2, and 6.8. Parallel imaging with reduction factors of up to 4.2 produced the images that retained sufficient image quality for speech imaging applications. In other words, the boundaries of the tongue, velum, and other articulators were clearly depicted. The $R = 6.8$ image

Table 2
Comparison of Average SNR Drop-Off in Three Volunteers

		Subject 1	Subject 2	Subject 3
Age/Sex		34/M	24/F	33/M
Size (A-P/S-I)[a]		11.0 cm/9.1 cm	9.3 cm/6.6 cm	12.2 cm/9.1 cm
	ROI	SNR_{ROI}/SNR_{pw}	SNR_{ROI}/SNR_{pw}	SNR_{ROI}/SNR_{pw}
1	Upper lip	7.1	3.1	6.4
2	Lower lip	7.0	3.0	8.0
3	Front tongue	3.9	1.9	3.2
4	Mid tongue	2.6	1.5	2.0
5	Back tongue	2.2	1.4	1.6
6	Palate	3.8	1.4	3.9
7	Velum	2.0	1.1	1.4
8	Pharyngeal wall	1.0	1.0	1.0

Average SNR was measured in three volunteers using the 16-channel coil. Eight regions of interest were identified in 2D midsagittal images with 1.88 × 1.88 × 2.50 mm^3 spatial resolution, obtained without the use of parallel imaging. Note the relatively less steep SNR drop-off from the small female subject.
[a]A-P size was measured as the distance from the lower lip to the pharyngeal wall, and S-I size was measured as the distance from the hard palate to the glottis.

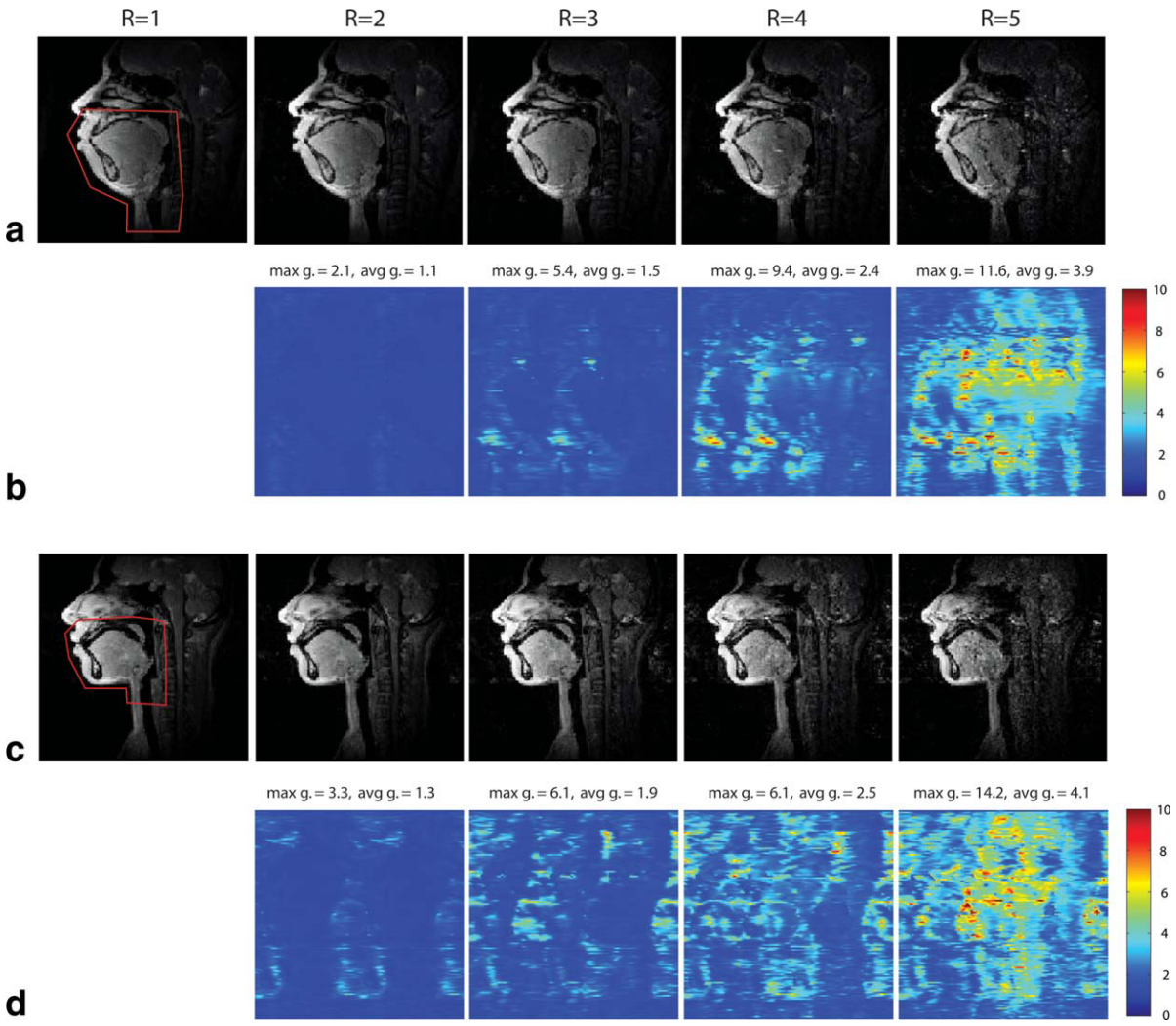

FIG. 3. 2D midsagittal image reconstruction using 1D SENSE. The direction of undersampling was A-P. SENSE reconstructed images with a spatial resolution of 1.88 × 1.88 × 2.50 mm^3 are compared with respect to reduction factors from 2 to 5 for the **(a)** Subject 1 and **(c)** Subject 2. Corresponding g-factor maps are shown for the **(b)** Subject 1 and **(d)** Subject 2. The mean and maximum *g*-factors shown were computed from the ROIs indicated by the red contours of the $R = 1$ images in (a) and (c). [Color figure can be viewed in the online issue, which is available at wileyonlinelibrary.com.]

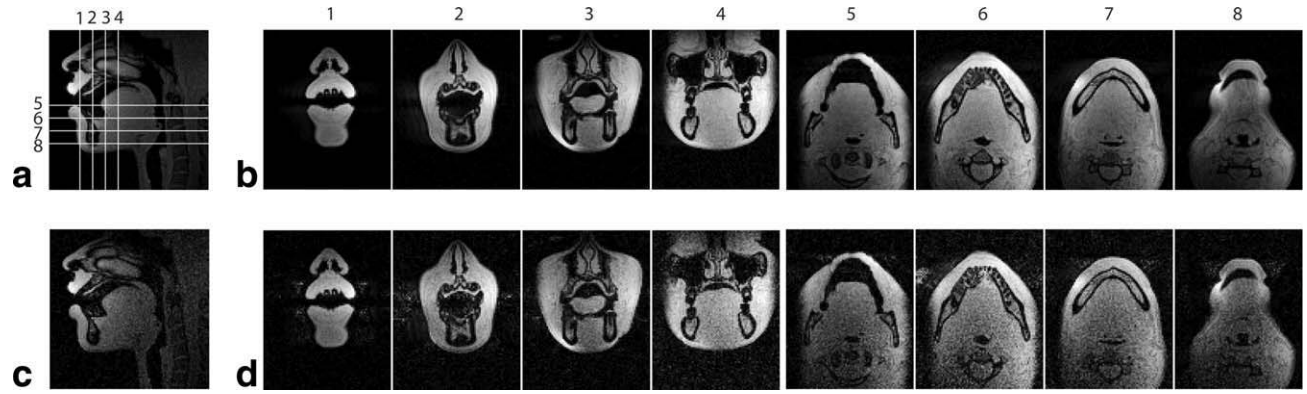

FIG. 4. 3D image reconstruction using 2D SENSE. The directions of undersampling were A-P and R-L. Fully sampled 1.25 mm isotropic resolution 3D data set was acquired in open-mouthed position during 54 sec scan. Retrospective undersampling was performed with a regular undersampling factor of 6, where 2-fold acceleration was along R-L direction and 3-fold acceleration was along A-P direction. Reformatted midsagittal images are shown for **(a)** SENSE $R = 1$, and **(c)** SENSE $R = 6$. Eight representative coronal and axial images are shown for **(b)** SENSE $R = 1$ and **(d)** SENSE $R = 6$. Air-tissue boundaries that are relevant to the vocal tract shape measurement are well defined in all the SENSE $R = 6$ images.

(see Fig. 5a) exhibited poor depiction of these boundaries because of lower image SNR. The constriction between the tongue blade and the alveolar ridge is seen during the utterance of /i/ (the solid arrows in Fig. 5b). Also, the constriction between the tongue tip and the alveolar ridge is seen during the utterance of /S/ (the hollow arrows in Fig. 5b).

DISCUSSION

The 16-channel coil produced acceptable image quality in static upper airway imaging with conventional Cartesian SENSE from a rate-4 in 1D undersampling and a rate-6 in 2D undersampling. This opens up new opportunities for upper airway MRI with improved spatial resolution. For example, a 1.25 mm isotropic resolution 3D imaging of the vocal tract is achievable with a rate-6 conventional SENSE and a 9 sec scan time. This is already a substantial improvement over the recently reported accelerated 3D sustained vocal tract imaging that utilized the single-channel birdcage coil and achieved a $1.5 \times 1.5 \times 2.0$ mm^3 resolution and 7 sec scan time using compressed sensing (5). Higher acceleration than a rate-6

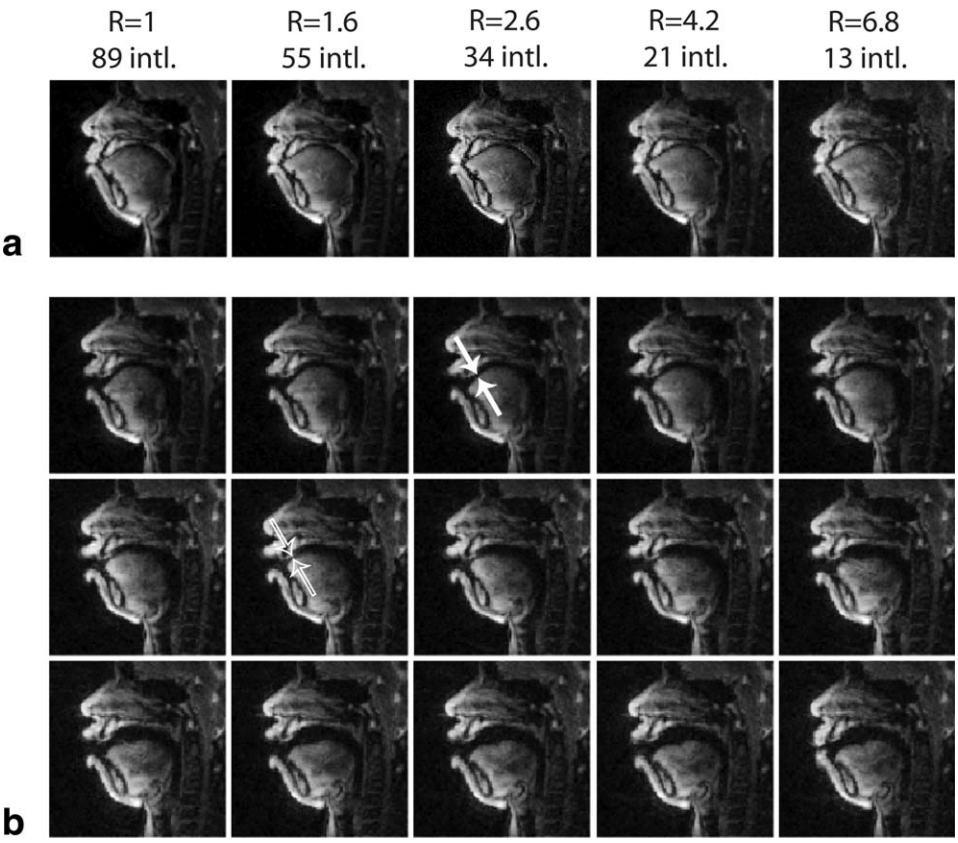

FIG. 5. 2D image reconstruction of the dynamics of vocal tract shaping using spiral SENSE. **(a)** Comparison of spiral SENSE images from a single representative frame. For the evaluation of SENSE reconstruction performance under different reduction factors, the frame was chosen from the data acquired when the subject (Subject 1) was stationary. Spatial aliasing was substantially reduced for all the SENSE reconstructed images. The $R = 6.8$ image exhibited relatively lower image SNR in the posterior regions of the upper airway (e.g., velum and pharyngeal wall). **(b)** Dynamic frames that represent the subject's utterance of "ee shop." The $R = 4.2$ SENSE reconstruction was used to generate the image frames with its frame update rate of 44 msec. The frame sequence is ordered from the top left to the bottom right.

may be achievable by using advanced image reconstruction methods such as the combined use of compressed sensing and parallel imaging (19).

The localized sensitivity with the 16-channel coil enables spiral imaging with a smaller FOV, and leading to better spatio-temporal resolution compared to what is possible with the 8-channel NV coil. As reduction factor increases to 6.8 in the spiral parallel imaging, noticeable SNR degradation occurred from the iterative SENSE reconstruction. Iterative SENSE with an explicit regularization (e.g., total variation regularization) may be beneficial since it mitigates noise amplification and preserves the edges of the air-tissue interface. It is worth noting that the use of SENSE-based non-Cartesian parallel imaging requires: (1) Full FOV image acquisition (including the brain that is not our region-of-interest) for estimating coil sensitivity. (2) Extrapolation to estimate coil sensitivity in image regions occupied by air. Data inconsistency due to motion of the articulators can also lead to inaccuracy in data fitting term and degrade image quality. As an alternative, k-space based parallel imaging approaches, such as non-Cartesian GRAPPA (20), do not require the explicit estimation of coil sensitivity maps and may be more robust in practice.

Compared to the 8-channel NV coil array, which has large-sized coil elements, coil calibration may be more difficult with the 16-channel coil, which has a larger number of smaller diameter elements. As such, coil sensitivities are more highly localized and rapidly moving anatomy (e.g., lips, tongue tip) that is close to the coil elements has a strong signal contribution.

In coil design there is also much room for improvement. For example, future designs can benefit from: rearrangement of the coil elements to reduce the *g*-factor in its worst places, better coverage of the lower airway with additional coil elements, better coverage of the pharyngeal wall with a few large coils around the back of the head, access for a respirator or mask covering the face and nose for experiments related to airway collapse (21), and rearrangement of the coil elements to allow for easier opening of the lower jaw. It is also worth of investigating the benefit of using higher channel counts (32 or more) for even higher acceleration.

CONCLUSIONS

This novel 16-channel coil array provides rate-4 acceleration to 2DFT midsagittal imaging, rate-6 acceleration to 3DFT imaging, and rate-4.2 acceleration to 2D spiral midsagittal imaging of the upper airway. This will lead to either higher spatial resolution or reduced scan time in capturing a 3D vocal tract shape during sustained sound production. This coil has the potential to allow for improved spatio-temporal resolution in dynamic upper airway MRI studies of swallowing and normal/disordered speech.

ACKNOWLEDGMENTS

The authors would like to thank the Rehabilitation Medicine Department of the NIH Clinical Center for providing the 16-channel UA coil, and Dr. Gloria Chi-Fishman for guidance during the initial development of the coil for tongue imaging. The authors acknowledge the support and collaboration of the Speech Production and Articulation knowledge (SPAN) group at the University of Southern California.

REFERENCES

1. Shellock FG, Schatz CJ, Julien P, Steinberg F, Foo TK, Hopp ML, Westbrook PR. Occlusion and narrowing of the pharyngeal airway in obstructive sleep apnea: evaluation by ultrafast spoiled GRASS MR imaging. Am J Roentgenology 1992;158:1019–1024.
2. Arens R, McDonough JM, Costarino AT, Mahboubi S, Tayag-Kier CE, Maislin G, Schwab RJ, Pack AI. Magnetic resonance imaging of the upper airway structure of children with obstructive sleep apnea syndrome. Am J Respir Crit Care Med 2001;164:698–703.
3. Hartl DM, Albiter M, Kolb F, Luboinski B, Sigal R. Morphologic parameters of normal swallowing events using single-shot fast spin echo dynamic MRI. Dysphagia 2003;18:255–262.
4. Narayanan SS, Alwan AA, Haker K. An articulatory study of fricative consonants using magnetic resonance imaging. J Acoust Soc Am 1995;98:1325–1347.
5. Kim YC, Narayanan SS, Nayak KS. Accelerated three-dimensional upper airway MRI using compressed sensing. Magn Reson Med 2009;61:1434–1440.
6. Narayanan S, Nayak K, Lee S, Sethy A, Byrd D. An approach to real-time magnetic resonance imaging for speech production. J Acoust Soc Am 2004;115:1771–1776.
7. Byrd D, Harris KS. Identifying and evaluating apraxic speech deficits using magnetometry. Proceedings of the 16th International Congress of Phonetic Sciences, Saarbrucken, Germany 2007.
8. Sutton BP, Conway C, Bae Y, Brinegar C, Liang Z-P, Kuehn DP. Dynamic imaging of speech and swallowing with MRI. Proceedings of IEEE Eng in Med and Biol Soc, Minneapolis, MN, USA, 2009, pp 6651–6654.
9. Byrd D, Tobin S, Bresch E, Narayanan SS. Timing effects of syllable structure and stress on nasals: a real-time MRI examination. J Phon 2009;37:97–110.
10. Breyer T, Echternach M, Arndt S, Richter B, Speck O, Schumacher M, Markl M. Dynamic magnetic resonance imaging of swallowing and laryngeal motion using parallel imaging at 3 T. Magn Reson Imaging 2009;27:48–54.
11. Roemer PB, Edelstein WA, Hayes CE, Souza SP, Mueller OM. The NMR phased array. Magn Reson Med 1990;16:192–225.
12. Ohliger MA, Sodickson DK. An introduction to coil array design for parallel MRI. NMR Biomed 2006;19:300–315.
13. Kellman P, McVeigh ER. Image reconstruction in SNR units: a general method for SNR measurement. Magn Reson Med 2005;54:1439–1447.
14. Pruessmann KP, Weiger M, Scheidegger MB, Boesiger P. SENSE: sensitivity encoding for fast MRI. Magn Reson Med 1999;42:952–962.
15. Winkelmann S, Schaeffter T, Koehler T, Eggers H, Doessel O. An optimal radial profile order based on the golden ratio for time-resolved MRI. IEEE Trans Med Imaging 2007;26:68–76.
16. Pruessmann KP, Weiger M, Bornert P, Boesiger P. Advances in sensitivity encoding with arbitrary k-space trajectories. Magn Reson Med 2001;46:638–651.
17. Qu P, Zhong K, Zhang B, Wang J, Shen GX. Convergence behavior of iterative SENSE reconstruction with non-Cartesian trajectories. Magn Reson Med 2005;54:1040–1045.
18. Uecker M, Zhang S, Voit D, Karaus A, Merboldt K-D, Frahm J. Real-time MRI at a resolution of 20 ms. NMR Biomed 2010;23:986–994.
19. Lustig M, Pauly JM. SPIRiT: Iterative self-consistent parallel imaging reconstruction from arbitrary k-space. Magn Reson Med 2010;64: 457–471.
20. Heidemann RM, Griswold MA, Seiberlich N, Kruger G, Kannengiesser SAR, Kiefer B, Wiggins G, Wald LL, Jakob PM. Direct parallel image reconstructions for spiral trajectories using GRAPPA. Magn Reson Med 2006;56:317–326.
21. Colrain I, Nayak KS, Nielsen JF. Real-time MRI of upper airway collapse during inspiratory loading. Proceedings of the 14th Annual Meeting of ISMRM, Seattle, WA, USA 2006 (abstract 2417).